CMOS Integrated 32 A/W and 1.6 GHz Avalanche Photodiode Based on Electric Field-Line Crowding

S. S. Kohneh Poushi, B. Goll, *Member, IEEE*, K. Schneider-Hornstein, M. Hofbauer, *Member, IEEE*, and Horst Zimmermann, *Senior Member, IEEE*

***Abstract*— This letter presents a new Si CMOS linear-mode avalanche photodiode (APD) based on an electric field distribution formed by field-line crowding. In this structure, a spherical avalanching electric field is enforced by field-line crowding due to the curvature of the half-sphere cathode (n-well). The electric field extends radially and, therefore, the entire low-doped epitaxial layer serves as charge collection zone. This APD can provide high responsivity and bandwidth due to its thick absorption zone and drift-based carrier transport. Measurements using a 675 nm laser source at 200 nW optical power show a maximum bandwidth of 1.6 GHz while the responsivity is 32 A/W. In addition, a maximum responsivity of 3.05×10^3 A/W at 5 nW optical power is achieved. Due to the high avalanche gain, large bandwidth, and CMOS compatibility without any process modification, this APD is a promising optical detector for many applications.**

***Index Terms*— Avalanche photodiode (APD), field-line crowding, CMOS integrated photodetector, spherical avalanching field.**

I. Introduction

DETECTION of low-power, high-bandwidth optical signals is required in many optical systems such as optical communication, time-of-flight sensing, and biomedical imaging. Due to the inherent gain of linear-mode avalanche photodiodes (APDs), the use of integrated APDs instead of standard pin photodiodes is interesting [1]–[3]. APDs fabricated in a complementary metal-oxide semiconductor (CMOS) technology have the advantages of low production cost and integration capability with electronic circuitry for read-out and signal processing.

Common design approaches towards integrated Si CMOS APDs are based on p^+/n-well [4]–[6] and n^+/p-well [7], [8] junctions. These devices demonstrate inevitably a trade-off between bandwidth and responsivity for the long-wavelength range (i.e. red and near-infrared light). The structures with a thin depleted absorption region provide a high bandwidth due to a shorter drift time of charge carriers. However, the carriers generated underneath the thin absorption region do not contribute to the output current resulting in a low responsivity [9].

Manuscript received 13 July 2022; accepted 27 July 2022. Date of publication 1 August 2022; date of current version 16 August 2022. This work was supported by the Austrian Science Fund (FWF) under Grant P34649. *(Corresponding author: S. S. Kohneh Poushi.)*

The authors are with the Institute of Electrodynamics, Microwave and Circuit Engineering, Vienna University of Technology, 1040 Vienna, Austria (e-mail: saman.kohneh@tuwien.ac.at).

Color versions of one or more figures in this letter are available at https://doi.org/10.1109/LPT.2022.3195191.

Digital Object Identifier 10.1109/LPT.2022.3195191

APDs based on the concept of separate absorption and multiplication regions were introduced to provide high responsivity, however, the bandwidth of such structures is generally limited by carrier drift time in a thick absorption zone [10], [11]. In Reference [10] a maximum responsivity of 2.7×10^4 A/W for 5-nW optical power at 670 nm, and a maximum bandwidth of 850 MHz (R = 20 A/W) were reported. The speed-optimizing technique of modulation doping was used to improve the bandwidth to 1.25 GHz while maintaining the same responsivity [12]. However, such bandwidth was achieved at a reverse voltage of 115 V with the drawback that the capability of the diode isolation from the circuits on the same chip is not good enough. Reference [13] presented a new structure called current-assisted avalanche photodiode (CA-APD) with separate absorption and multiplication regions. This APD employs two electrodes at the surface with different potentials to create an electric field for drifting the photogenerated electrons in the detection volume towards the central multiplication region. A bandwidth of 275 MHz and 13 A/W responsivity at 830 nm was reported for this APD.

Recently, [14] and [15] introduced an electric field-line crowding based single-photon avalanche photodiode (SPAD) fabricated in a CMOS process. They had to customize, i.e. to modify, the fabrication process to use a shallow n-type implant at the silicon surface between cathode and anode to redistribute the electric field just below the silicon/silicon dioxide interface at the surface of the device. A silicon photomultiplier (SiPM) used also a SPAD exploiting the field-line crowding effect [16]. But transistors cannot be fabricated in the special SiPM detector process.

In this work, we employ the field-line crowding concept to design a new APD fabricated in a standard CMOS process without any process modification. The APD uses a small spherical avalanching n-well/p- epi junction at the center and a thick volume in the p- epitaxial layer with lower electric field around the avalanching region as absorption zone (Fig. 1). This APD achieves a maximum responsivity of 3.05×10^3 A/W at 5 nW optical power and a maximum bandwidth of 1.6 GHz (R = 32 A/W) at 200 nW optical power for the wavelength of 675 nm.

II. APD Structure and TCAD Simulation

Fig. 1 shows the structure and doping regions of the APD fabricated in 0.18 μm high-voltage CMOS technology. The cathode comprises an n^+ region with a radius of 0.37 μm embedded in an n-well region with a radius of 0.6 μm.

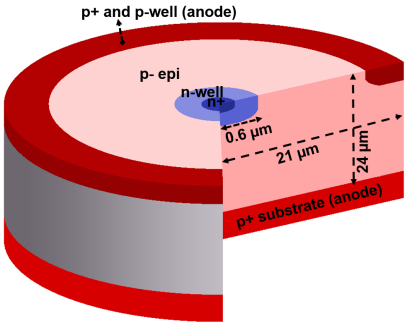

Fig. 1. Schematic 3-D drawing of the n^+/n-well field crowding based Si CMOS APD (not to scale).The APD is covered by an isolation and passivation stack.

The cathode is concentrically enclosed by a p+ region (anode) with an inner radius of 19 μm. These regions are formed on a low p-doped epitaxial layer (p- epi) with a thickness of $\sim$24 μm and a doping concentration of $\sim 1.5 \times 10^{13}$ cm^{-3}. The p+ substrate is also used as anode. The APD is covered by the standard isolation and passivation stack. At the operating voltage, a space-charge region is formed at the junction of the n-well and p- epi region and its electric field distribution can be derived from Gauss's law. The derivation assumes that the highly doped cathode is much smaller than the other device dimensions and that it forms an abrupt transition into the intrinsic layer. Based on these assumptions, the electric field distribution in the p- epi layer is approximately [15]

$$\mathrm{E}(d) \approx \frac{(V_r + V_{bi})d_n}{d^2}, \tag{1}$$

where d_n is the cathode's radius, V_r is the operation voltage, and V_{bi} is the built-in voltage. Accordingly, the electric field peak is at the n-well/p- epi junction and decays by moving radially away from the center at a rate of d^{-2} as can be seen in Fig. 2 (b). At the p-substrate contact ring, i. e. at r = 19 μm, the electric field has still a magnitude of 3500 V/cm. Below the cathode at r = 0 μm just at the transition to the p+ substrate (in a depth of 20 μm), the magnitude of the electric field is still 5 kV/cm. In "diagonal" direction along the dashed line in Fig. 2(a), is still 3 kV/cm at 25 μm away from the origin of coordinates. This high electric field strength enables fast carrier drift from a half sphere with a radius of about 20 μm, whereas the APD of [10] had only an about 8 μm thick drift region [17], which limited the bandwidth by a small contribution of slow carrier diffusion to 850 MHz.

The n-well radius is one of the most important factors in determining the breakdown voltage as the electric field strength depends on the curvature of the n-well/p- epi junction. A smaller cathode radius leads to a sharper field peak. Accordingly, the breakdown and operating voltages decrease by reducing the cathode radius [15], [16].

TCAD simulations were preformed using Silvaco's ATLAS [18] to obtain the electric field distribution inside the structure. When the APD is biased in linear mode (below the breakdown voltage), a spherical high electric field region is formed near the cathode (around n-well region) which acts as the multiplication region. The width of the multiplication region is $\sim$0.9 μm. The electric field extends towards the

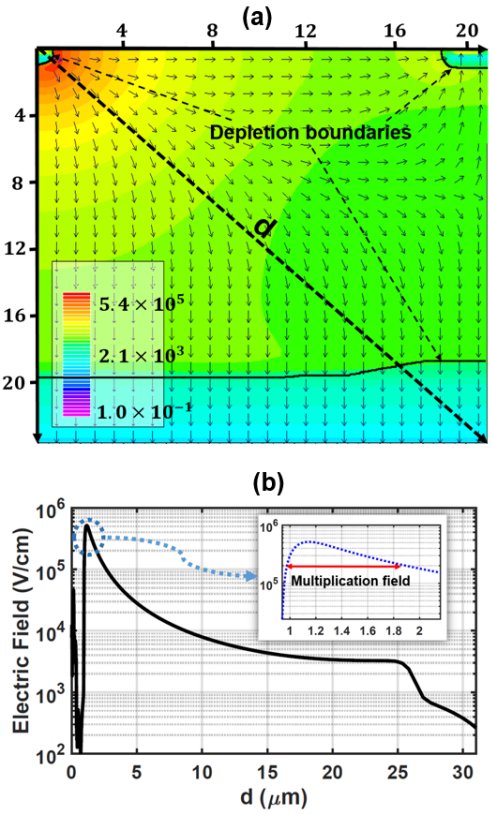

Fig. 2. (a) 2D Plot of the electric field within the APD obtained by TCAD simulations for a reverse voltage of 69 V. Arrows indicate the local electric field direction. (b) Radial cross-section of the electric field in the structure along the dashed line in sub-figure (a).

substrate and towards the surface anode but decreases by moving radially away from the center (Fig. 2(b)). Accordingly, the generated electrons and holes in the entire volume of the epitaxial layer are promptly separated by the electric field, and then the electrons are accelerated in the direction opposite to the electric field vector arrows (Fig. 2(a)) towards the multiplication region (cathode). Such a large thickness of the absorption region and the drift-based carrier transport improve the detector's responsivity and speed performance for long wavelengths, respectively.

It is worth mentioning that this APD can be integrated with electronic circuitry on the same silicon chip as the used high voltage CMOS technology provides different wells to isolate the MOS transistors down to substrate potentials of -100 V.

III. Measurement Results

Here the APD is evaluated in terms of some key performance features such as gain, responsivity, and bandwidth. The measurements have been performed on wafer at 25 °C temperature regulated by a thermo chuck.

A. Currents, Gain and Responsivity

Fig. 3 illustrates the dark current and the photocurrent of the APD at different optical powers measured using an electrometer (Keysight B2987A). A 675 nm single-mode fiber with

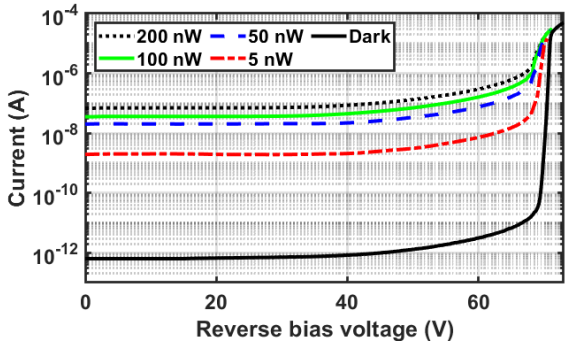

Fig. 3. Measured dark and photo currents as a function of reverse bias voltage for different optical powers (5 nW, 50 nW, 100 nW, 200 nW).

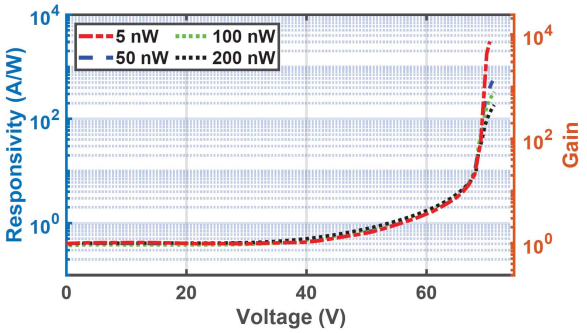

Fig. 4. Responsivity (left) and gain (right) as a function of reverse bias voltage for different optical powers.

a core diameter of 5 μm coupled with an optical attenuator was used to provide different optical power. A calibrated optical power meter was used to measure the optical power on the device under test. The dark characteristics shows the breakdown voltage of 70.7 V where the dark current reaches 1 μA. Based on the photocurrent characteristics, the gain and responsivity as a function of reverse bias voltage are obtained from the following equations:

$$\text{Gain(V)} = \frac{\text{I(V)} - \text{I}_{\text{dark}}\text{(V)}}{\text{I(V}_0\text{)} - \text{I}_{\text{dark}}\text{(V}_0\text{)}}, \tag{2}$$

$$\text{Responsivity(V)} = \frac{\text{I(V)} - \text{I}_{\text{dark}}\text{(V)}}{\text{Optical Power}}, \tag{3}$$

where I represents currents, and V_0 stands for a reference voltage for unity gain.

Fig. 4 shows the gain and responsivity for 5 nW, 50 nW, 100 nW, and 200 nW optical powers. An unamplified responsivity of 0.41 A/W at $\text{V}_0 = 1$ V and a maximum responsivity of 3.05×10^3 A/W at V = 70.5 V are achieved, which are comparable to the results reported in Reference [10]. It is observed that the gain and responsivity are independent of the optical power in a wide voltage range (below 68.94 V) where the gain is lower than 76.52 and the responsivity is lower than 30.6 A/W. However, with increasing voltage, the gain and responsivity achieved for higher optical power are smaller compared to that for lower optical powers because of the saturation effect of the multiplication process at high optical powers due to partial screening of the electric field by many charges [19]. Table I contains the responsivity and gain for different optical powers at $V_r = 70.5$ V.

TABLE I

DEPENDENCY OF RESPONSIVITY AND GAIN ON THE OPTICAL POWER AT $V_r = 70.5$ V

Parameters	5 nW	50 nW	100 nW	200 nW
Responsivity (A/W)	3.05×10^3	397	234	130
Gain	7.47×10^3	980	610	325

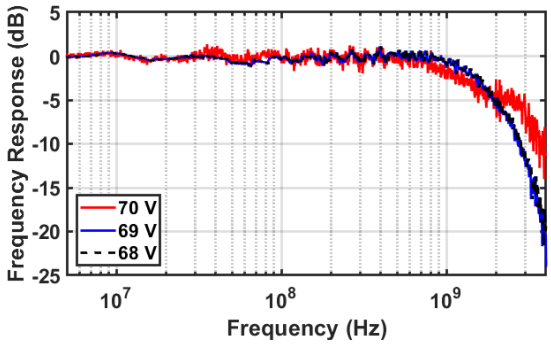

Fig. 5. Normalized frequency responses at 200 nW optical power for different operating voltages.

B. Frequency Response and Bandwidth

Fig. 5 shows the normalized frequency responses of the APD at an optical power of 200 nW ($\lambda = 675$ nm) for different gains, which were measured using a vector network analyzer (Rohde&Schwarz ZNB8). A high voltage bias-tee (Freq$\sim$5 MHz-18GHz) is used to supply the diode and send the RF signal back to the network analyzer.

The maximum bandwidth of 1.6 GHz was measured at $V_r = 69$ V, corresponding to the gain and responsivity of 80 and 32 A/W, respectively. This APD shows a bandwidth enhancement of $\sim$ 90% compared to the results reported in [10]. This is due to the large radius of the half-sphere high-field region of about 20 μm compared to a thickness of the drift region in [10] of only about 8μm, which lead to a small contribution of slow carrier diffusion.

It is observed that the bandwidths at $V_r = 68$ V and $V_r = 69$ V show almost the same value because the electric field in the absorption region, and consequently, the drift time doesn't vary significantly. The responsivity and gain of 10 A/W and 25 are repectively achieved at $V_r = 68$ V. The bandwidth drops at $V_r = 70$ V which is because of the avalanche build-up time. In fact, since the avalanche process takes time, the higher multiplication factor increases the avalanche build-up time and thus limits the bandwidth. This effect can be clearly seen in Fig. 5 for the multiplication factor of $\sim$300 (R = 115 A/W) which results in a bandwidth of 1.28 GHz. However, as the optical power is 200 nW, the avalanche build-up time effect is not significantly dominant, and thus the bandwidth drop is low. The presented APD achieves the gain-bandwidth product of 128 GHz and 384 GHz,

TABLE II
PERFORMANCE COMPARISON OF LINEAR-MODE APDS (SM-APD: APD WITH SEPARATE ABSORPTION AND MULTIPLICATION REGION; CA-APD: CURRENT ASSISTED APD)

Parameters	Ref [10]	Ref [9]	Ref [6]	Ref [13]	Ref [12]	This work
Technology	0.35 μm	45 nm	0.25 μm	0.35 μm	0.35 μm	0.18 μm
Structure	n^+/p-well SM-APD	Double p-well/ deep p-well APD	p^+/n-well APD	p^+/n-well CA-APD	n^+/p-well SM-APD	n^+/n-well field crowding based APD
Area	Round r=60 μm	20×20 μm^2	10×10 μm^2	40×40 μm^2	Round r=60 μm	Round r=21 μm
Operating voltage	63 V	20.8 V	12.2 V	68 V	115 V	69 V
Optical power	500 nW	100 μW	1 mW	2 μW	2 μW	200 nW
Wavelength	670 nm	850 nm	850 nm	830 nm	670 nm	675 nm
Responsivity	20.5 A/W	0.56 A/W	0.2 A/W	13.17 A/W	20.5 A/W	32 A/W
Gain	50	23	16.7	43.9	50	80
Bandwidth	850 MHz	8.4 GHz	5.6 GHz	275 MHz	1.25 GHz	1.6 GHz
Gain-bandwidth product	42.5 GHz	193.2 GHz	93.5 GHz	12 GHz	62.5 GHz	128 GHz

corresponding to the gain and bandwidth of G = 80, BW = 1.6 GHz, and G = 300, BW = 1.28 GHz, respectively.

Table II shows a comparison of the key performance parameters of the presented APD with various silicon photodetectors fabricated in standard CMOS technologies. The field-crowding APD reduces the optical power and increases the avalanche gain as well as the bandwidth compared to the other APDs. Furthermore, the breakdown voltage of the suggested APD is comparable to that of the field-crowding SPAD of 67.3 V [14].

IV. CONCLUSION

To the best knowledge of the authors, the first electric field-line crowding linear-mode APD is presented. It is shown that at the operating voltage, a spherical multiplication region is formed around the n-well region (cathode). The electric field extends to the detection zone, but gradually decreases with moving radially away from the center. This results in a thick fully depleted absorption zone in which the photogenerated electrons drift towards the cathode. Due to such a thick absorption zone, an unamplified and a maximum responsivity of 0.41 A/W and of 7.47 $\times$ 10^3 A/W, respectively, at 5 nW optical power are achieved, which are comparable to the results reported in [10]. However, the maximum bandwidth of 1.6 GHz is measured which shows $\sim$90% improvement compared to that reported in [10].

ACKNOWLEDGMENT

The authors would like to thank A. Zimmer from XFAB for technical support and D. Sommer for fabrication support.

REFERENCES

[1] E. Kamrani, F. Lesage, and M. Sawan, "Low-noise, high-gain transimpedance amplifier integrated with SiAPD for low-intensity near-infrared light detection," *IEEE Sensors J.*, vol. 14, no. 1, pp. 258–269, Jan. 2014.

[2] O. Shcherbakova, L. Pancheri, N. Massari, G.-F. D. Betta, and D. Stoppa, "Linear-mode gain-modulated avalanche photodiode image sensor for time-of-flight optical ranging," *IEEE Trans. Electron Devices*, vol. 63, no. 1, pp. 145–152, Jan. 2016.

[3] D. Milovancev, T. Jukic, N. Vokic, P. Brandl, B. Steindl, and H. Zimmermann, "VLC using 800-μm diameter APD receiver integrated in standard 0.35–μm BiCMOS technology," *IEEE Photon. J.*, vol. 13, no. 1, pp. 1–13, Feb. 2021.

[4] K. Iiyama, H. Takamatsu, and T. Maruyama, "Hole-injection-type and electron-injection-type silicon avalanche photodiodes fabricated by standard 0.18 μm CMOS process," *IEEE Photon. Technol. Lett.*, vol. 22, no. 12, pp. 932–934, Jun. 15, 2010.

[5] L. Pancheri, G.-F. D. Betta, and D. Stoppa, "Low-noise avalanche photodiode with graded junction in 0.15 μm CMOS technology," *IEEE Electron Device Lett.*, vol. 35, no. 5, pp. 566–568, May 2014.

[6] M.-J. Lee, J.-M. Lee, H. Rucker, and W.-Y. Choi, "Bandwidth improvement of CMOS-APD with carrier-acceleration technique," *IEEE Photon. Technol. Lett.*, vol. 27, no. 13, pp. 1387–1390, Jul. 1, 2015.

[7] S. Nayak, A. H. Ahmed, A. Sharkia, A. S. Ramani, S. Mirabbasi, and S. Shekhar, "A 10-Gb/s –18.8 dBm sensitivity 5.7 mW fully-integrated optoelectronic receiver with avalanche photodetector in 0.13-μm CMOS," *IEEE Trans. Circuits Syst. I, Reg. Papers*, vol. 66, no. 8, pp. 3162–3173, Aug. 2019.

[8] M.-J. Lee and W.-Y. Choi, "A silicon avalanche photodetector fabricated with standard CMOS technology with over 1 THz gain-bandwidth product," *Opt. Exp.*, vol. 18, no. 23, pp. 24189–24194, Nov. 2010.

[9] W. Zhi, Q. Quan, P. Yu, and Y. Jiang, "A 45 nm CMOS avalanche photodiode with 8.4-GHz bandwidth," *Micromachines*, vol. 11, no. 1, p. 65, Jan. 2020.

[10] B. Steindl, R. Enne, S. Schidl, and H. Zimmermann, "Linear mode avalanche photodiode with high responsivity integrated in high-voltage CMOS," *IEEE Electron Device Lett.*, vol. 35, no. 9, pp. 897–899, Sep. 2014.

[11] B. Steindl, W. Gaberl, R. Enne, S. Schidl, K. Schneider-Hornstein, and H. Zimmermann, "Linear mode avalanche photodiode with 1-GHz bandwidth fabricated in 0.35-μm CMOS," *IEEE Photon. Technol. Lett.*, vol. 26, no. 15, pp. 1511–1514, Aug. 1, 2014.

[12] R. Enne, B. Steindl, and H. Zimmermann, "Speed optimized linear-mode high-voltage CMOS avalanche photodiodes with high responsivity," *Opt. Lett.*, vol. 40, no. 19, pp. 4400–4403, 2015.

[13] G. Jegannathan, H. Ingelberts, S. Boulanger, and M. Kuijk, "Current assisted avalanche photo diodes (CAAPDs) with separate absorption and multiplication region in conventional CMOS," *Appl. Phys. Lett.*, vol. 115, no. 13, Sep. 2019, Art. no. 132101.

[14] E. Van Sieleghem *et al.*, "A near-infrared enhanced silicon single-photon avalanche diode with a spherically uniform electric field peak," *IEEE Electron Device Lett.*, vol. 42, no. 6, pp. 879–882, Jun. 2021.

[15] E. Van Sieleghem *et al.*, "A backside-illuminated charge-focusing silicon SPAD with enhanced near-infrared sensitivity," *IEEE Trans. Electron Devices*, vol. 69, no. 3, pp. 1129–1136, Mar. 2022.

[16] E. Engelmann, W. Schmailzl, P. Iskra, F. Wiest, E. Popova, and S. Vinogradov, "Tip avalanche photodiode—A new generation silicon photomultiplier based on non-planar technology," *IEEE Sensors J.*, vol. 21, no. 5, pp. 6024–6034, Mar. 2021.

[17] B. Steindl, "Einzelphotonen-lawinendioden für integrierbare optische empfänger," Ph.D. dissertation, Inst. Electrodyn., Microw. Circuit Eng., Vienna Univ. Technol., Vienna, Austria, 2019.

[18] *Silvaco Atlas User's Manual*. Accessed: 2022. [Online]. Available: https://www.silvaco.com

[19] A. Karar *et al.*, "Investigation of avalanche photodiodes for EM calorimeter at LHC," CERN Accelerating Sci., Tech. Rep., SCAN-9510272, 1995.